

Article

Adsorption of Brilliant Green Dye onto a Mercerized Biosorbent: Kinetic, Thermodynamic, and Molecular Docking Studies

Andra-Cristina Enache ¹, Corneliu Cojocaru ^{1,*}, Petrisor Samoila ¹, Victor Ciornea ², Roxana Apolzan ³,
Georgeta Predeanu ⁴ and Valeria Harabagiu ¹

¹ Laboratory of Inorganic Polymers, “Petru Poni” Institute of Macromolecular Chemistry, 41A Grigore Ghica Voda Alley, 700487 Iasi, Romania; humelnicu.andra@icmpp.ro (A.-C.E.); hvaleria@icmpp.ro (V.H.)

² Faculty of Biology and Chemistry, “Ion Creanga” State Pedagogical University, 1 Ion Creangă Street, MD-2069 Chisinau, Moldova

³ SC Cosfel Actual SRL, 95-97 Grivitei Street, 010705 Bucharest, Romania

⁴ Research Center for Environmental Protection and Eco-Friendly Technologies (CPMTE), University Politehnica of Bucharest, 1 Polizu Street, 011061 Bucharest, Romania; gpredeanu@gmail.com

* Correspondence: cojocaru.corneliu@icmpp.ro

Abstract: This study reports the valorization of pistachio shell agricultural waste, aiming to develop an eco-friendly and cost-effective biosorbent for cationic brilliant green (BG) dye adsorption from aqueous media. Pistachio shells were mercerized in an alkaline environment, resulting in the treated adsorbent (PS_{NaOH}). The morphological and structural features of the adsorbent were analyzed using scanning electron microscopy, Fourier transform infrared spectroscopy, and polarized light microscopy. The pseudo-first-order (PFO) kinetic model best described the adsorption kinetics of the BG cationic dye onto PS_{NaOH} biosorbents. In turn, the equilibrium data were best fitted to the Sips isotherm model. The maximum adsorption capacity decreased with temperature (from 52.42 mg/g at 300 K to 46.42 mg/g at 330 K). The isotherm parameters indicated improved affinity between the biosorbent surface and BG molecules at lower temperatures (300 K). The thermodynamic parameters estimated on the basis of the two approaches indicated a spontaneous ($\Delta G < 0$) and exothermic ($\Delta H < 0$) adsorption process. The design of experiments (DoE) and the response surface methodology (RSM) were employed to establish optimal conditions (sorbent dose (SD) = 4.0 g/L and initial concentration (C_0) = 10.1 mg/L), yielding removal efficiency of 98.78%. Molecular docking simulations were performed to disclose the intermolecular interactions between the BG dye and lignocellulose-based adsorbent.

Keywords: pistachio shells; biosorbent; brilliant green; optimization; molecular docking



Citation: Enache, A.-C.; Cojocaru, C.; Samoila, P.; Ciornea, V.; Apolzan, R.; Predeanu, G.; Harabagiu, V. Adsorption of Brilliant Green Dye onto a Mercerized Biosorbent: Kinetic, Thermodynamic, and Molecular Docking Studies. *Molecules* **2023**, *28*, 4129. <https://doi.org/10.3390/molecules28104129>

Academic Editor: Eric Guibal

Received: 21 April 2023

Revised: 15 May 2023

Accepted: 15 May 2023

Published: 16 May 2023



Copyright: © 2023 by the authors. Licensee MDPI, Basel, Switzerland. This article is an open access article distributed under the terms and conditions of the Creative Commons Attribution (CC BY) license (<https://creativecommons.org/licenses/by/4.0/>).

1. Introduction

The consequences of urbanization, rapid population growth, and the concomitant need for economic development have led to the significant pollution of natural waters. Therefore, the development of sustainable methods for water and wastewater treatment is imperative nowadays [1]. Along with the progress of the industrial sector, most natural-origin dyes have been supplanted by synthetic dyes as a result of rising demands and prohibitive costs associated with extracting natural compounds [2]. Therefore, synthetic dyes are considered a worrisome polluting factor in wastewater, as they are widely used in various industries (e.g., textiles, pharmaceuticals, cosmetics, paper, plastic, paint, and leather) [2–4]. It is estimated that the textile industry alone utilizes more than 10^7 kg of dye per year worldwide, of which 10^6 kg is discharged into water streams [5]. As a consequence, synthetic dyes from wastewater have led to an increase in waterborne diseases worldwide, and implicitly in morbidity and mortality [6–8].

Cationic dyes are recognized to be more harmful than anionic dyes, possessing high tinctorial values (1 mg/L) [9]. Among these is brilliant green (BG), a triphenylmethane dye with widespread usage in human and veterinary medicine when used in low-concentration solutions (e.g., antiseptic, antifungal, and anthelmintic properties) [10,11]. Additionally, BG is extensively used as a coloring agent for textile materials and paper (approximately 1 kg/ton of paper), as well as in the rubber and plastic industries [12–14]. However, this dye is classified as highly toxic, causing harmful effects in humans when in contact with the skin and eyes, by inhalation, or by ingestion (the probable lethal dose is 50–500 mg/kg) [15,16]. It has been demonstrated that the toxic effect of BG dye found in green paper towels (which are frequently used in hospitals, factories, and other facilities) involves transdermal penetration of the skin, even during brief exposure intervals (30–300 s) [17]. Similar effects were obtained for the consumption of fish contaminated with this dye, due to its illicit use in aquaculture [17]. Despite being hazardous to aquatic organisms, BG is easily integrated into aquatic systems due to its high solubility (100 g/L) [15,18]. Moreover, its extreme volatility pollutes the atmosphere, and its decomposition products (sulfur and nitrogen oxides, as well as carbon dioxide) are damaging to the environment [13–15,18]. Thus, removing this dye from wastewater has become a major challenge.

In the last few decades, different treatment technologies have been performed in order to remove BG dye from aqueous media, such as biological [19] and oxidative [20] processes, electrocoagulation [21], sono-catalytic degradation [22], membrane separation [23], and adsorption [7]. Weighing the advantages and limitations of the mentioned methods, adsorption on the solid surface of the dye is one of the most effective methods in terms of simplicity and low costs [10]. In addition, for the adsorption process of BG to become economically feasible, researchers have focused on biodegradable, renewable, sustainable, easily available, and low-cost adsorbents, such as guava seeds [5], banana peels [7], kaolin [10], bagasse fly ash [12], sawdust [13], rice straw [15], medlar nucleus [17], Saklikent mud [18], cashew nut shell [24], or acorn-based [25] materials. The adsorption technique has also been shown to be remarkable in the removal of other dye pollutants from aqueous solutions [4,8,26–28]. For example, environmentally friendly modifications to lignocellulosic materials such as walnut shells resulted in improved adsorption capabilities of two other cationic dyes with expanded medicinal applications (crystal violet and methylene blue) [26]. Furthermore, lignin-based magnetic biochar demonstrated significant Congo red removal efficiency in simulated wastewater [27], as well as excellent selective adsorption capability for methylene blue in binary, ternary, and quaternary dye systems [28]. However, for the treatment of contaminated waters, biosorbents derived from agricultural waste represent a valuable, affordable, and ecological alternative [29]. Pistachio (*Pistacia vera* L.) is considered one of the most valuable agricultural products from an economic standpoint in countries such as Iran, the US, Turkey, and Syria, which are responsible for almost 90% of the worldwide production [30,31]. The global demand for pistachio is increasing, mainly due to its beneficial impacts on human health (rich in nutrients and bioactive compounds) [32,33]. Considering their wide production and the shell/nut ratio of about 45%, large amounts of organic waste biomass are usually discharged by the processing industries to landfills (around 30 million tons/year) [8,31]. Furthermore, the chemical composition of pistachio shells, which contains abundant functional groups primarily provided by cellulose (40%), hemicellulose (25%), and lignin (16%) [8,34], can easily provide high added value and improved properties for dye adsorption processes.

The synthesis of sulfuric-acid-based activated carbon using pistachio shells was studied for methylene blue and brilliant green adsorption [35]. Due to its high adsorption capacity and increased surface area, activated carbon is one of the most widely utilized adsorbents; however, its high cost makes this technique uneconomical for commercial applications [10]. In this context, this study aimed to create a novel, simple, cost-effective, and environmentally friendly modified adsorbent based on pistachio shells for the removal of carcinogenic brilliant green from aqueous solutions. As far as we know, this is the first study to report the adsorption of brilliant green on a pistachio shell biosorbent obtained

through simple grinding and mercerization processes. In addition to the characterization of the biosorbent from a physicochemical point of view, this study also reports the optimization of the separation process, as well as molecular docking simulations (to disclose the adsorption mechanism). Moreover, the thermodynamic parameters of adsorption were determined using two approaches: the classical one and the one based on the modified Langmuir isotherm proposed by Azizian et al. [36]. Both approaches take into account the saturation concentration of the investigated sorbate and lead to the same conclusions regarding the thermodynamics of the process.

2. Results and Discussion

2.1. Modification of Pistachio Shells by Mercerization (PS_{NaOH})

To provide a cost-effective and practical solution for removing harmful cationic brilliant green dye from wastewater, pistachio shell waste was employed. This material was chosen for two reasons. First, large amounts of biomass are commonly discarded as agro-waste, leading to significant environmental concerns [31]. Second, pistachio shells possess diverse functional groups, such as cellulose (hydroxyl) and lignin content (hydroxyl, carbonyl, methoxyl, and carboxyl [34]). These functional groups make surface modification possible, which in turn can enable the acquisition of new properties that are suitable for cationic dye adsorption procedures [37].

The alkaline treatment of pistachio shells was selected to improve the adhesive properties of the surface, providing a rough topography as a result of the removal of natural and artificial impurities from the surfaces of the pistachio shells [38]. Furthermore, this method is commonly used to activate cellulose by immersing the lignocellulosic biomass in NaOH solutions with concentrations ranging from 5 to 7% [39]. In this study, a concentration of 5% (NaOH) was used to reduce the environmental impact; also, the mercerized pistachio shells (PS_{NaOH}) were carefully washed with water to eliminate the excess of NaOH. In contrast to other chemical agents, the use of NaOH as a surface modification agent also has benefits, including lower corrosion capacity, a lower environmental impact during its life cycle, and economic viability [40].

2.2. Characterization of PS_{NaOH} Biosorbent

The surface morphological characteristics of the untreated and alkali-treated pistachio shells (PS and PS_{NaOH} , respectively) were assessed through scanning electron microscopy (SEM), as shown in Figure 1a,b. A heterogeneous surface characteristic of lignocellulosic materials was visible in the untreated PS sample, as illustrated in Figure 1a. Along with the rough texture of the PS sample, the presence of irregularly shaped impurities was noticed. These have been assigned mainly to the crushing and grinding process of pistachio shells, given that similar outcomes were also observed for walnut shells subjected to this process [26]. By comparison with the raw PS sample, the SEM image of PS_{NaOH} (Figure 1b) reveals the ability of the NaOH to remove the solid impurities from the biosorbent surface. Moreover, the alkali treatment of pistachio shells led to a smoother, wavy surface with the exposure of open pores, which are expected to increase the adsorption capacity of organic molecules.

FTIR spectroscopy was used to investigate the structural changes at the surface of the PS_{NaOH} biosorbent induced by the alkali treatment. As depicted in Figure 1c, the PS_{NaOH} biosorbent's spectrum was analyzed by comparison to the unmodified pistachio shell's (PS) spectrum. Due to their structural complexity, both spectra have been represented with breaks to highlight the two characteristic regions, namely the OH and CH stretching vibrations in the region of $3700\text{--}2700\text{ cm}^{-1}$ and the "fingerprint" region in the range of $1800\text{--}600\text{ cm}^{-1}$. The corresponding assignments for the absorption bands are detailed in Table S1. In brief, the spectrum of raw PS shows distinctive absorption bands, which indicate the presence of cellulose, hemicellulose, and lignin components [40–44]. As a consequence of the alkaline treatment, a series of spectral changes for PS_{NaOH} have been observed, as shown in Figure 1c. As expected, the partial dissolution of lignin and

hemicellulose occurred, as proven by the reduction in intensity and shifting of characteristic bands (1744 cm^{-1} and 1235 cm^{-1}). This can be explained by the cleavage of the aliphatic side chains in lignin and the breakage of the C–O–C bonds between the two monomers during hemicellulose hydrolysis in an alkaline solution [43]. Moreover, it was noted that the intensities of the peaks at 1421 cm^{-1} and 896 cm^{-1} had increased, indicating the higher content of cellulose in the treated samples. Similar findings were made when shea nut shells were alkali-treated [45]. Moreover, the increase in the intensities of the hydroxyl and carbonyl functionalities at the biosorbent surface (3343 cm^{-1} and 1030 cm^{-1}) is expected to improve the adsorption capacity of the PS_{NaOH} biosorbent.

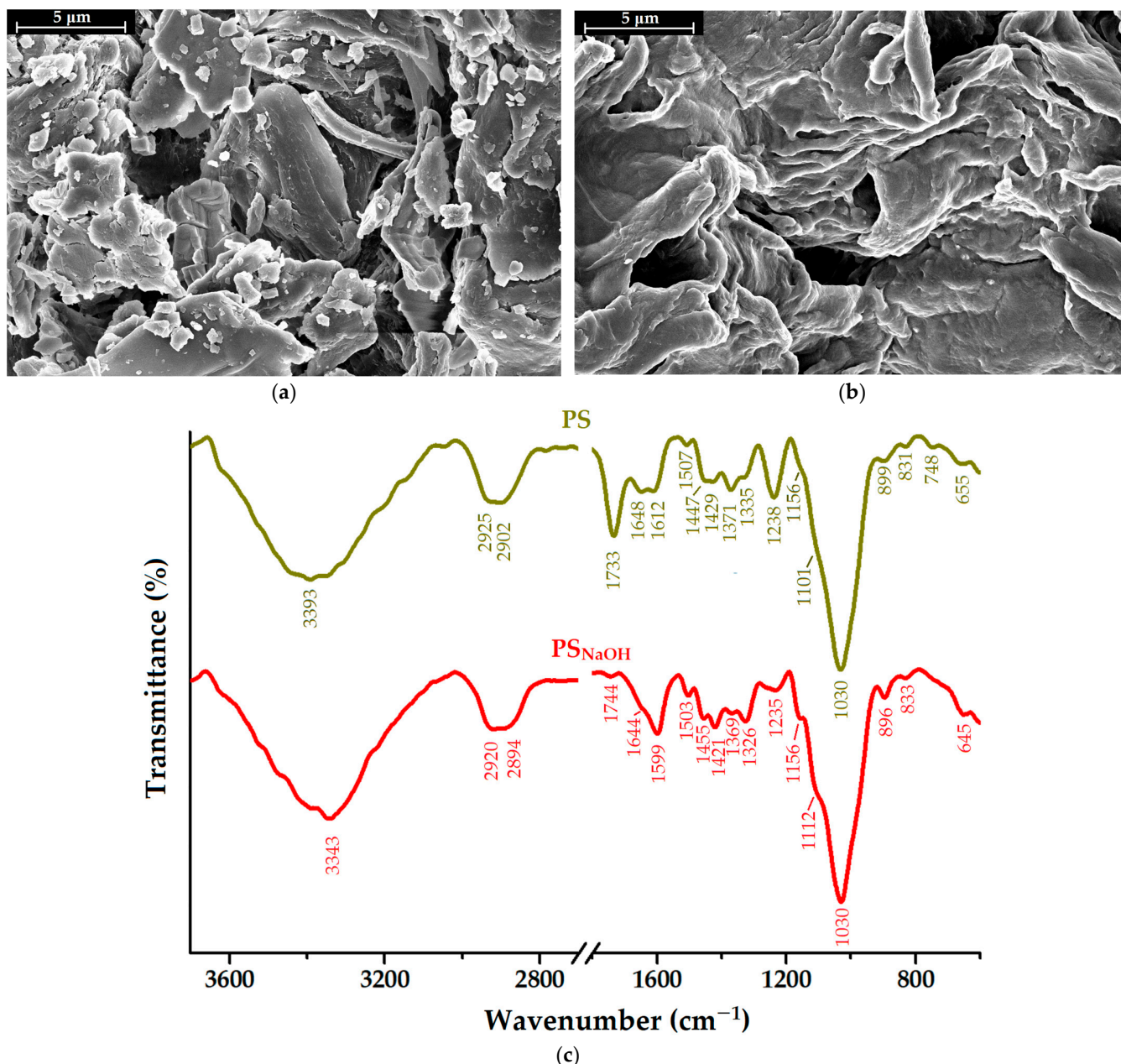


Figure 1. SEM images on the surface of (a) raw pistachio shell (PS) and (b) alkali-treated pistachio shell (PS_{NaOH}); (c) FTIR spectra of unmodified and alkali-treated pistachio shells (PS and PS_{NaOH} , respectively).

The water vapor sorption capacity (W%) of the PS_{NaOH} sample was slightly higher by comparison with the PS sample (as given in Table S2). In addition, the Brunauer–Emmett–

Teller kinetic (BET) and the Barrett–Joyner–Halenda (BJF) models were applied to calculate the specific surface area, the weight of water forming a monolayer, and the average pore size, respectively (following a protocol described in a previous work [46]). As shown in Table S2, the alkali treatment of pistachio shells led to a specific surface area of 253.2 m²/g and 323.5 m²/g for PS_{NaOH} and raw PS materials, respectively. However, one may say that the NaOH treatment of pistachio shells led to greater surface areas when compared with pistachio shells treated with H₂O₂ and NaOH or with HCl and HClO₄ [40]. In addition, the average pore size was observed to increase after NaOH treatment from 1.210 nm to 1.563 nm (Table S2). Besides these outcomes, the alkaline treatment has the benefit of cleaning the pistachio shells' surfaces of contaminants, which qualifies PS_{NaOH} for use in environmental applications.

2.3. Adsorption Studies of Brilliant Green onto PS_{NaOH} Biosorbent

2.3.1. Adsorption Kinetics and Isotherms

Brilliant green (BG) cationic dye revealed three absorbance wavelengths (318, 426, and 624 nm, respectively), as highlighted by Figure S1a in the Supplementary Materials. To ensure the accuracy of the data, the adsorption investigations employed the band at 624 nm. Thus, the concentration of BG in the solution was measured based on the calibration curve depicted (Figure S1b).

The BG adsorption kinetics onto the PS_{NaOH} biosorbent were evaluated, taking into consideration the influence of the contact time t (min) upon the adsorption capacity q_t (mg/g). Thus, Figure 2a shows an increase in adsorption capacity over time, corresponding to three stages [47]. The first stage is characterized by rapid adsorption (in the first 30 min), mainly due to the large number of available sites on the PS_{NaOH} surface. With the depletion of active adsorption sites, the second stage begins and is represented by a slower adsorption process (between 30 and 120 min). The BG molecules try to diffuse into the pores and are gradually adsorbed by the inner pores until equilibrium is established (>120 min). The plateau zone at equilibrium is achieved in this final stage due to the saturation of the biosorbent's reactive groups with BG molecules. A similar trend was observed by others when investigating BG adsorption onto chemically modified areca nut husk [48] and raw soybean milk residues [49].

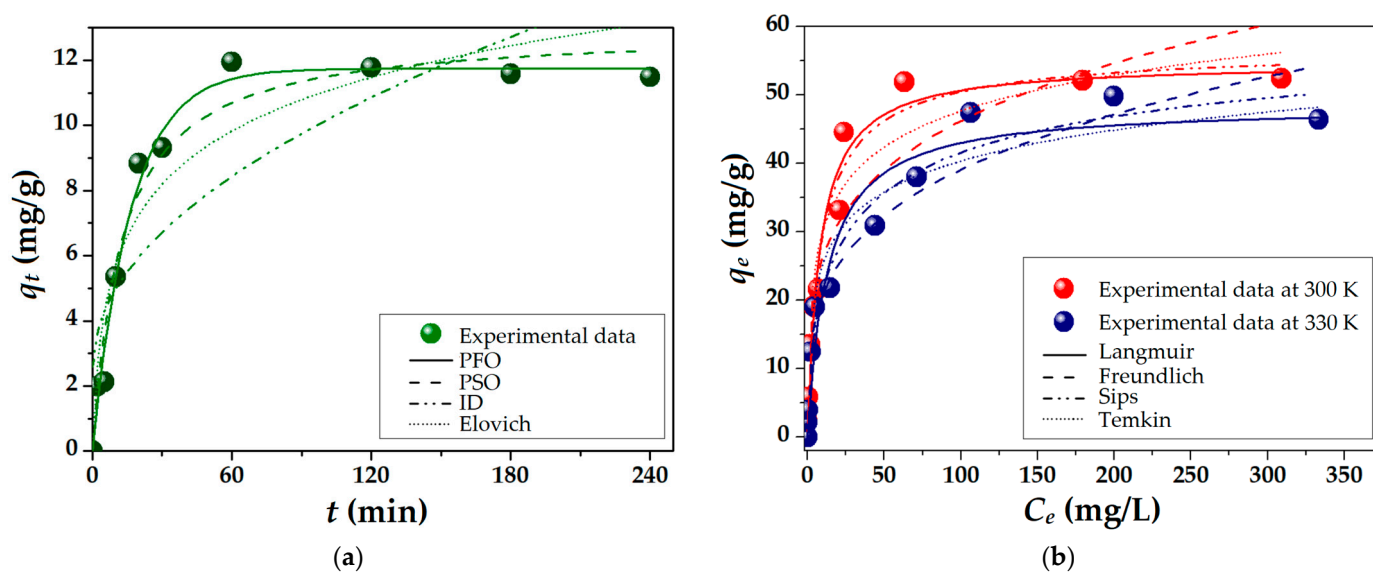


Figure 2. Adsorption of brilliant green (BG) onto PS_{NaOH} biosorbent: kinetic (a) and isotherm (b) studies (experimental data and mathematical models).

To investigate the rate of adsorption and better understand the adsorption mechanism, pseudo-first-order (PFO), pseudo-second-order (PSO), intra-particle diffusion (ID), and

Elovich kinetic models were employed (Figure 2a). The characteristic non-linear equations and parameters are given in Table S3 (Supplementary Materials). Furthermore, the chi-squared (χ^2) statistical test was used to determine the agreement between predicted and experimental data. Given the smallest value of χ^2 (Table S3) and the observations from Figure 2a, it is possible to conclude that the PFO model best describes the adsorption kinetics of BG onto the PS_{NaOH} biosorbent. The theoretical equilibrium adsorption capacity ($q_e^{(calc)} = 11.74$ mg/g) estimated by the PFO model is closest to the experimental result ($q_e^{(obs)} = 11.49$ mg/g) (see Table S3 in Supplementary Materials). These findings suggest that the adsorption mechanism of BG onto the PS_{NaOH} biosorbent is not predominantly based on diffusion (ID) [50].

The isotherm experiments were carried out at two temperatures (300 and 330 K) and represent the adsorption capacity at equilibrium (q_e , mg/g) as a function of the concentration of BG dye at equilibrium (C_e , mg/L), as illustrated in Figure 2b. As a result of the kinetic study (Figure 2a), the contact time was set at 240 min to ensure the adsorption equilibrium of the process. According to experimental isotherm data, the adsorption capacity at equilibrium (q_e) decreased with temperature, changing from 52.42 mg/g (at 300 K) to 46.42 mg/g (at 330 K). This might be attributed to the higher kinetic energy of the BG molecule when the temperature rises, which can reduce the electrostatic attraction and separate the solute from the biosorbent's surface [47]. These findings support the previously discussed kinetic results, corroborating that the increment in temperature does not cause the dye molecules to diffuse more inside the pores of the biosorbents. Other studies' outcomes revealed the opposite temperature dependency behavior [48,49]. However, the greater adsorption capacities of BG dye at moderate temperatures (closer to those found in the environment) may be advantageous when used in wastewater treatment applications.

To further explore the adsorption process of BG cationic dye on the PS_{NaOH} biosorbent, the experimental data were interpolated by the Langmuir, Freundlich, Sips, and Temkin isotherm models, as plotted in Figure 2b. The non-linear equations of these models and the obtained isotherm parameters are detailed in Table S4 (Supplementary Materials). According to the calculated chi-square (χ^2) values (see Table S4), the Sips isotherm model provided the best accuracy of data interpolation. Given that the Sips model combines the Langmuir (homogenous monolayer adsorption) and Freundlich (heterogeneous multilayer adsorption) models [51], it can be inferred that the BG molecules were adsorbed on the PS_{NaOH} surface in both manners, i.e., in homogeneous and heterogeneous layers.

In addition, the computed values of the R_L separation factor ($0 < R_L < 1$) and of the n_F Freundlich isotherm constant ($2 < n_F < 10$) support the assertion of a favorable adsorption process (see Table S4 in Supplementary Materials) [48]. However, the values for the constants of Langmuir (K_L), Freundlich (K_F), and Temkin (K_T), given in Table S4, are decreasing with increasing temperature, confirming the presence of a stronger interaction and improved affinity between the biosorbent surface and BG molecules at a lower temperature (of 300 K). To elucidate the adsorption mechanism (physical, ion exchange, or chemisorption [52]), the Dubinin–Radushkevich (D-R) model was applied, and the mean free energy (E_S , kJ/mol) was calculated (Table S4). Given the values of E_S ranging between 8 and 16 kJ/mol (~13 kJ/mol), it can be concluded that the adsorption process of BG cationic dye onto the PS biosorbent is mainly reliant on an ion-exchange mechanism between the surface acidic functional groups (e.g., $-\text{COO}^-$) of the adsorbent and positively charged nitrogen atoms from the brilliant green cationic dye.

The increased adsorption capacity of the PS_{NaOH} biosorbent with increasing concentrations of BG cationic dye in the aqueous solution was evidenced by polarized light microscopy (PoLM). As a triphenylmethane dye, brilliant green (Figure 3a) is known for its use as a fluorochrome in biological molecular labeling [53]. By comparison with the non-loaded (pristine) PS_{NaOH} biosorbent (Figure 3b), we observed the uniform adsorption of the BG dye onto the surface of the biosorbent (Figure 3c,d) after performing the isotherm study. One aspect to be noted is that after submerging the biosorbent in low concentrations of BG solution (10 mg/L for 240 min), the dye's absorption was reduced, but light could

still travel through the sample (Figure 3c). On the other hand, immersion in a concentrated solution with 500 mg/L of BG dye resulted in enhanced adsorption capacity (mg/g), which blocked the penetration of light (Figure 3d).

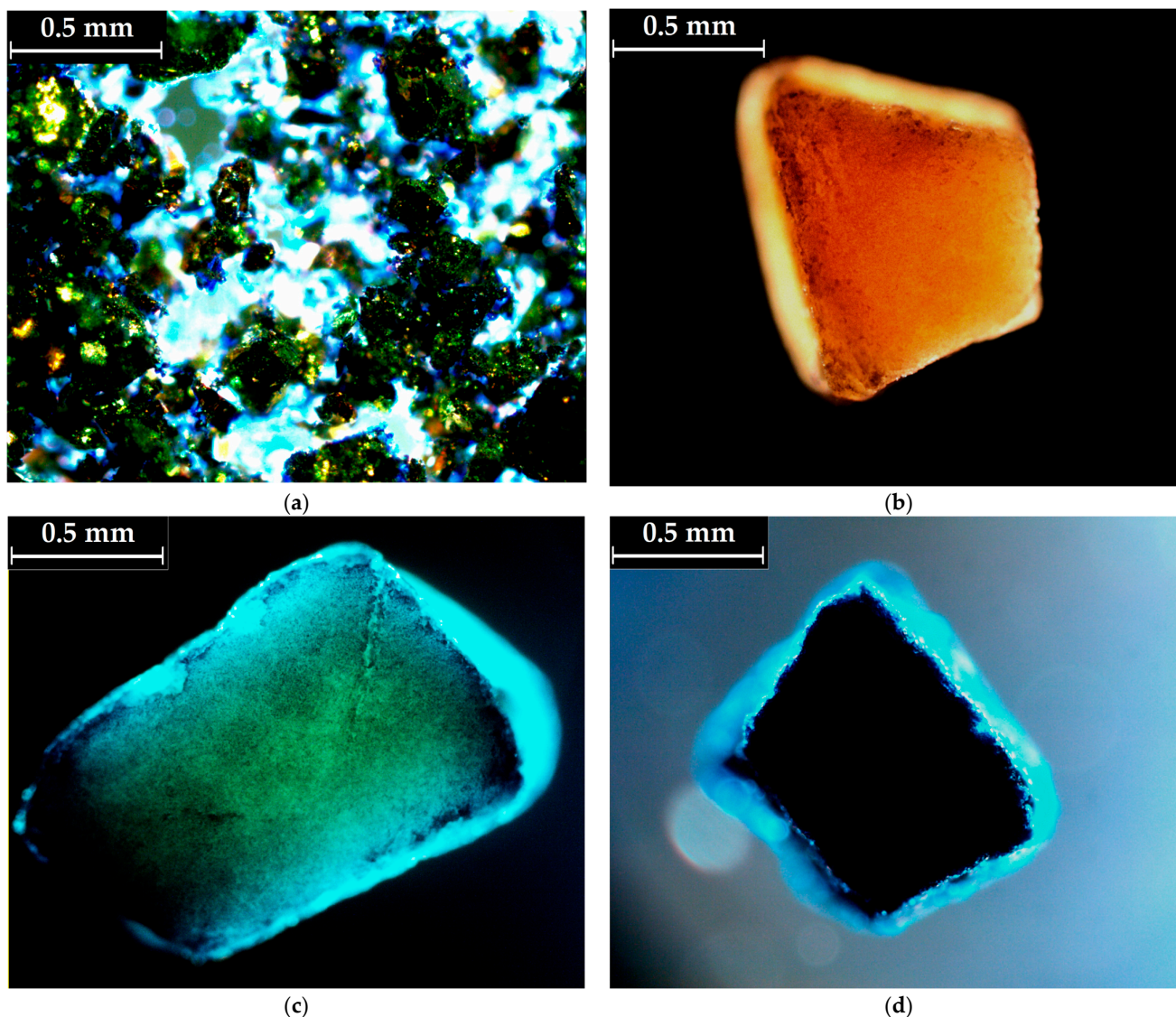


Figure 3. Polarization light images of (a) brilliant green solid particles (crystals); (b) non-loaded PS_{NaOH} grain; PS_{NaOH} grain after BG absorption from aqueous solutions with initial concentrations of (c) $C_0 = 10$ mg/L and (d) $C_0 = 500$ mg/L, respectively ($t = 240$ min).

In addition, a comparative literature review on the maximum adsorption capacities of brilliant green (BG) on different lignocellulosic materials was carried out. As shown in Table 1, higher adsorption capacities (80–250 mg/g) were obtained for activated-carbon-derived materials from guava seeds [5], pistachio shells [35], and cashew nut shells [24]. However, in recent decades, researchers have concentrated on replacing expensive activated carbons with low-cost modified lignocellulosic materials. Thus, cost-effective modifications were approached (cleaning with distilled water, hot water treatment, NaOH, Na_2CO_3 , or HCl treatment), yielding relevant adsorption capacities ranging from 18 to 59 mg/g [13,15,47,54–56]. Among these, sawdust from Indian Eucalyptus wood treated with NaOH had the highest value of BG adsorption (58.48 mg/g), followed by the PS_{NaOH} biosorbent employed in this investigation and similarly treated (54.74 mg/g). These findings support the use of PS_{NaOH} for the efficient removal of BG from aqueous solutions.

Table 1. Comparison of the maximum adsorption capacities (q_m) of different sorbent materials for BG cationic dye removal.

Sorbents Derived from Lignocellulosic-Based Biosorbents	Modifications	Maximum Adsorption Capacity (q_m , mg/g)	Ref.
Activated carbon (AC) from acorn	Carbonization in argon atmosphere	2.01	[25]
Activated carbon (AC) from guava seeds	Chemical activation with phosphoric acid	80.50	[5]
Activated carbon (AC) from pistachio shells	Chemical activation with sulfuric acid	151.52	[35]
Activated carbon (AC) from cashew nut shells	Chemical activation with potassium hydroxide	243.90	[24]
Peanut shells	Washing with water	19.92	[54]
Watermelon peels	Hot water treatment	25.00	[55]
Rice straw	Washed with water	30.68	[15]
Areca nut husk	NaOH treatment	18.21	[47]
Sawdust from Indian Eucalyptus wood	NaOH treatment	58.48	[13]
<i>Bambusa Tulda</i>	Na ₂ CO ₃ treatment	41.67	[56]
	HCl treatment	31.25	
	Distilled water washing	32.25	
Pistachio shells	NaOH treatment	54.74	This work

2.3.2. Thermodynamic Parameters

Assessing the principal thermodynamic parameters (such as Gibbs free energy, enthalpy, and entropy) provides useful information regarding the energetic changes that occur during the adsorption [26,57–61]. In order to ascertain these thermodynamic parameters, it is necessary to take into consideration the adsorption equilibrium constants at a minimum of two distinct levels of temperature (e.g., 300 and 330 K).

In this study, the adsorption equilibrium constant (K_{ad}) and consequently the thermodynamic parameters were estimated on the basis of two approaches. In the first approach, the adsorption equilibrium constant (K_{ad}) was approximated assuming the Langmuir equilibrium parameter K_L , which was converted from the (L/mg) unit to the (L/mol) unit according to Equation (1) [26]:

$$K_L \left(\frac{\text{L}}{\text{mol}} \right) = K_L \left(\frac{\text{L}}{\text{mg}} \right) \times 1000 \left(\frac{\text{mg}}{\text{g}} \right) \times M_w \left(\frac{\text{g}}{\text{mol}} \right) \quad (1)$$

where M_w (g/mol) is the molecular weight of the pollutant subjected to adsorption (i.e., BG dye). Afterward, the dimensionless adsorption equilibrium constant (K_{ad}) was estimated in conformity with Equation (2) [26,58]:

$$K_{ad} = K_L \left(\frac{\text{L}}{\text{mol}} \right) \times C_{ref} \left(\frac{\text{mol}}{\text{L}} \right) \times \frac{1}{\gamma} \quad (2)$$

where γ represents the activity coefficient ascertained on the basis of the ionic strength [36,58,60] and C_{ref} denotes the molar concentration of the reference state. Commonly, in the classical approach, the concentration of pollutant or adsorbate (in the reference state) is considered to be 1 M (i.e., $C_{ref} = 1 \text{ mol/L}$) [58]. Hence, when $C_{ref} = 1 \text{ M}$, the adsorption equilibrium constant K_{ad} (dimensionless) is numerically identical to the Langmuir constant K_L . However, there are real situations in which the reference concentration of 1 M cannot be used, because the water solubility of the considered pollutant is less than 1 M. In this particular situation, the reference concentration is approximated to the saturated solution

(C_S) [36]. For example, the water solubility of the brilliant green (BG) dye is about 100 g/L (0.2072 mol/L). Thus, in the first approach, we calculated the adsorption equilibrium constant (K_{ad}) by using Equation (2) and considering the saturated solution as the reference concentration (that is, $C_{ref} = C_S$, mol/L). Regarding the activity coefficient (γ), this was calculated by the Davis relationship [58].

In the second approach, the adsorption equilibrium constant (K_{ad}) was considered to be equal to the dimensionless equilibrium parameter K_{ML} from the revised Langmuir isotherm model (i.e., $K_{ad} = K_{ML}$). This revised Langmuir isotherm model was proposed and validated in 2018 by Azizian and co-workers [36], and the revised equation can be expressed as

$$q_e = \frac{q_m K_{ML} C_e}{(C_S - C_e) + K_{ML} C_e} \quad (3)$$

where q_e (mg/g) is the adsorption capacity at equilibrium, q_m (mg/g) is the model parameter representing the maximum adsorption capacity as a monolayer, C_e (mg/L) is the concentration of the pollutant (or adsorbate) at equilibrium, C_S (mg/L) is the solubility of the pollutant (or adsorbate) in water (a saturated solution) and K_{ML} (dimensionless) is the modified Langmuir constant representing the ratio between the elementary rate constants of adsorption (k_a) and desorption (k_d)—that is, $K_{LM} = k_a/k_d$. The key difference between the modified Langmuir constant K_{LM} and the classical Langmuir constant K_L relies on the fact that K_{LM} is a dimensionless quantity, whereas K_L has specific units (L/mg) [36]. Therefore, the K_{LM} constant can be directly employed in thermodynamic calculations, without additional mathematical transformations [36].

Thus, two approaches, (1) $K_{ad} = K_L \times C_S \times \gamma^{-1}$ and (2) $K_{ad} = K_{ML}$, were further used to assess the thermodynamic parameters. Consequently, the changes in the Gibbs free energy of adsorption (ΔG) were computed as [26,36,58,60]

$$\Delta G = -R_g T \ln(K_{ad}) \quad (4)$$

where K_{ad} is the equilibrium constant of adsorption (dimensionless), T is the absolute temperature (K), and R_g is the universal gas constant ($R_g = 8.314$ J/(K·mol)). The variation in the enthalpy (ΔH) for the adsorption process was calculated by considering the isochore equation of Van't Hoff, which may be expressed by Equation (5) [60]:

$$\Delta H = \frac{-R_g \ln\left(\frac{K_{ad,T_2}}{K_{ad,T_1}}\right)}{\frac{1}{T_2} - \frac{1}{T_1}}, \quad (5)$$

where T_1 and T_2 are two different values of temperature; consequently, K_{ad,T_1} and K_{ad,T_2} are adsorption equilibrium constants established for the corresponding temperatures. The modification of the entropy (ΔS_{ad}) was assessed using the following thermodynamic equation [36,58,59]:

$$\Delta S = \frac{\Delta H_{ad} - \Delta G_{ad}}{T}, \quad (6)$$

The computed values of the thermodynamic parameters resulting from the two approaches are reported in Table 2. Both approaches revealed similar results, i.e., the calculated thermodynamic parameters by different methods were close in value (Table 2). It should be mentioned herein that the calculations according to the second approach ($K_{ad} = K_{ML}$) were faster since there was no need to compute the ionic strength and the activity coefficient separately. As summarized in Table 2, the negative values for the Gibbs free energy ($\Delta G_{ad} < 0$) indicated that the studied adsorption processes were spontaneous (exergonic). Moreover, the ΔG_{ad} values less than -20 kJ/mol might suggest the presence of the ion-exchange phenomenon [61]. The calculated values of the enthalpies were found to be negative ($\Delta H_{ad} < 0$), indicating the exothermic nature of the studied adsorption processes. As reported in Table 2, the entropy change was positive ($\Delta S_{ad} > 0$) for all cases,

highlighting the increase in randomness (at the solid–liquid interface) that contributed to the spontaneity of the process.

Table 2. Thermodynamic parameters for the adsorption of BG dye onto PS_{NaOH} biosorbent; thermodynamic calculations performed via two approaches.

Approach ¹	T (K)	K_{ad}	ΔG_{ad} (kJ/mol)	ΔH_{ad} (kJ/mol)	ΔS_{ad} (J/K·mol)
(1) $K_{ad} = K_L \times C_S \times \gamma^{-1}$	300 K	1.779×10^4	−24.411	−12.602	39.363
	330 K	1.124×10^4	−25.592		39.364
(2) $K_{ad} = K_{ML}$	300 K	1.236×10^4	−23.502	−12.681	36.070
	330 K	7.786×10^3	−24.584		36.069

¹ K_{ad} is the adsorption equilibrium constant, K_L is the Langmuir equilibrium parameter (L/mol); C_S denotes the concentration of the saturated solution; $\gamma = 0.695$; K_{ML} is the dimensionless equilibrium parameter from the revised Langmuir isotherm model.

The revised Langmuir isotherm model (given by Equation (3)) was used to interpolate the experimental data obtained in the isotherm study (Section 2.3.1) and the isotherm curves are evidenced in Figure S2, while the corresponding parameters are detailed in Table S5 in the Supplementary Materials. As a result, the theoretical values for the maximum adsorption capacity (q_m , mg/g) obtained by this approach are very close to those obtained by the classical Langmuir approach. However, it should be mentioned that the revised Langmuir isotherm model provides better data interpolation (smaller chi-square (χ^2) values) for experiments conducted at low temperatures (e.g., 300 K).

2.3.3. Design of Experiments (DoE) for Data-Driven Modeling and Optimization

The effectiveness of an adsorption process in wastewater treatment is largely determined by the optimal conditions [62]. In this study, the synergetic effect of two key factors, influencing the adsorption performance, was explored to establish the optimal conditions, i.e., (1) sorbent dose (SD , g/L) and (2) initial pollutant concentration C_0 (mg/L). For adsorption process optimization, the design of experiments (DoE) and the response surface methodology (RSM) approach were adopted [63,64]. Brilliant green dye (BG) was employed as a target organic pollutant dissolved in the contaminant water, and the adsorption process was investigated in a systematic way. In this respect, a central composite design (CCD) of the rotatable type was applied for experimentation (Table 3). As detailed in Table 3, the operating variables (factors) are reported in terms of actual values (SD and C_0) and coded values (x_1 and x_2). The experimental design listed in Table 3 involved 11 experimental runs. For each run, both factors (SD and C_0) were varied simultaneously, recording the process response (Y , %). The central runs (9–11) from CCD (Table 3) were carried out at the midpoints of factor intervals to assess the reproducibility of the experiment. Thus, the reproducibility test was conducted in triplicate, as reported for runs 9, 10, and 11 (Table 3), which were carried out in the center of the experimental region. According to the reproducibility assay (runs 9, 10, and 11), the average value for the removal efficiency was equal to $93.68 \pm 0.47\%$, which corresponded to an adsorption capacity of 33.48 ± 0.18 mg/g. Hence, the reproducibility error was less than 0.55%.

Based on the numerical data given in Table 3 (experimental matrix), a mathematical model was built using the multiple regression method [63,64]. In this regard, the multiple regression computations were performed using the Design Expert (v.10) program. The developed model, with two variables, is of the polynomial type and contains the following terms: (1) main (linear) effects, (2) curvature (quadratic), and (3) pairwise (two-variable) interaction. The model can be expressed in terms of coded variables (x_1 and x_2) as follows:

$$\hat{Y} = 39.68 + 20.33x_1 - 16.37x_2 + 13.53x_1x_2 - 16.07x_1^2 - 5.93x_2^2 \quad (7)$$

subjected to : $-1.414 \leq x_j \leq 1.414$; ($j = 1, 2$)

Table 3. Central composite design (rotatable type) adopted for experimentation of BG dye removal from aqueous solutions by adsorption using PS_{NaOH} as an adsorbent.

Run	Sorbent Dose		Initial Concentration of BG Dye		Removal Efficiency (Response), Determined after 120 Min of Contact Time
	Coded x_1	Actual SD , g/L	Coded x_2	Actual C_0 , mg/L	
1	−1	1.00	−1	50.0	91.40
2	+1	6.00	−1	50.0	96.12
3	−1	1.00	+1	250.0	25.57
4	+1	6.00	+1	250.0	84.42
5	−1.414	1.17	0	150.0	23.83
6	+1.414	6.83	0	150.0	93.88
7	0	4.00	−1.414	8.6	98.02
8	0	4.00	+1.414	292.4	60.25
9	0	4.00	0	150.0	93.15
10	0	4.00	0	150.0	93.84
11	0	4.00	0	150.0	94.06

The resulting polynomial model (Equation (7)) was checked, regarding whether it was significant, by using the statistical test based on the analysis of variance (ANOVA) [63]. The main ANOVA statistical estimators are given in Table S6. As a result, the F-value of 26.51 and a small p -value of 0.0013 indicated a significant model from a statistical point of view. Consequently, the model can be used to navigate the design space through simulations. The value of the multiple correlation coefficient R^2 (0.963) disclosed that about 96% of the variability in the sum of squares could be explained by the factors under consideration. After applying the mathematical substitution technique, the final empirical model with natural factors can be written as follows:

$$\hat{Y} = 40.56 + 32.15 \times SD - 0.26 \times C_0 + 0.07 \times SD \times C_0 - 4.02 \times SD^2 - 5.39 \times 10^{-4} \times C_0^2 \quad (8)$$

$$\text{subjected to : } 1.17 \leq SD \leq 6.83 \text{ (g/L); } 8.6 \leq C_0 \leq 291.4 \text{ (mg/L)}$$

The estimations given by the data-driven model are shown in Figure 4. As highlighted in Figure 4a, there is reasonable agreement between the experimental data (actual response) and model estimations, since the data are scattered around the bisector (45° straight line). Figure 4b reveals that the main effect of the initial concentration (C_0) factor is negative, while the main effect of the SD factor is positive with respect to the estimated response (\hat{Y} , %). In other words, the greater the C_0 factor, the lower the estimated response. In turn, as the sorbent dose factor (SD) increases, the estimated response becomes higher (Figure 4b). The quadratic effects of both factors induce curvature in the response surface. In addition, there is an interaction effect between factors SD and C_0 . In accordance with this two-factor interaction effect, the influence of the SD factor is more noticeable at higher values of the initial concentration of BG dye. Instead, the effect of the C_0 factor is more pronounced at smaller amounts of sorbent (Figure 4b).

Lastly, the constructed mathematical model was employed for process optimization. To this end, the numerical optimization was carried out by means of the direct search algorithm included in the Design Expert program. The model-based optimization results suggested the following optimal conditions: $SD = 4.0$ g/L and $C_0 = 10.1$ mg/L. For these optimal conditions, the computed response was equal to $\hat{Y} = 104.98\%$ (the predicted value), while the observed removal efficiency (recorded after 120 min of contact time) was $Y = 98.78\%$ (the actual value). The difference of about 6.20% represented the residual error between the model and the experiment. Note that the actual value of the response

(98.78%) determined for the optimal conditions was the highest value compared to any value reported in Table 3.

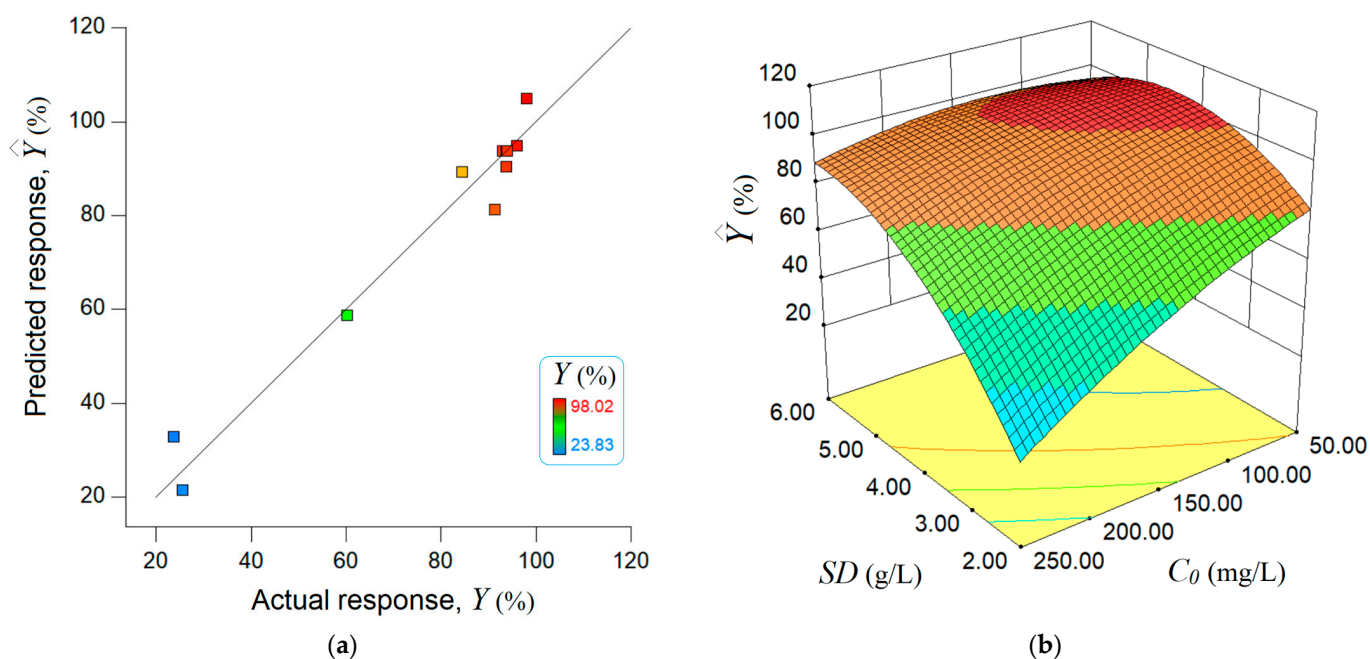


Figure 4. Data-driven modeling outcomes given by RSM: (a) agreement between experimental data and model predictions; (b) response surface of the estimated removal efficiency (\hat{Y} , %) dependent on the experimental factors, i.e., sorbent dose SD and initial pollutant concentration C_0 .

Following the determination of the optimal adsorption conditions for BG on the PS_{NaOH} biosorbent, the influence of the pH on the removal efficiency of BG was evaluated. Lower removal efficiency values were found at more acidic or alkaline pH levels, as indicated in Figure S3 (Supplementary Materials), as compared to the maximum value corresponding to the natural pH ≈ 6 (used in all the experiments by dissolving BG powder in distilled water). Once the pH is lowered (towards pH 2), additional H^+ ions compete for the available adsorption sites (negatively charged) with the positively charged BG molecules, resulting in a decrease in dye removal efficiency [28]. By contrast, more adsorption sites (negatively charged) become accessible as the pH of the solution rises. These adsorption sites produce an electrostatic attraction with the cationic dye molecules, increasing the removal efficiency. Such a scenario was observed at pH 6, followed by decreasing removal efficiency for pH > 8 , when the opposite effect (electrostatic repulsion) might occur [28,48]. However, it should be mentioned that PS_{NaOH} exhibited excellent BG adsorption ability with removal efficiency higher than 90% in a wide pH range (4–8), similar to the wastewater pH range.

In addition, the influence of coexisting anions (Cl^- , NO_2^- , and SO_4^{2-}), cations (Na^+ , Ca^{2+} , and Fe^{2+}), or organic matter (humic acid) on BG removal onto the PS_{NaOH} biosorbent was assessed [27,28]. As depicted in Figure S4 in the Supplementary Materials, the addition of different salts led to a decrease in BG removal efficiency from 98.87% (in the absence of supplemental ions) to values in the range of 34.52–86.57% (in the presence of coexisting ions) and to 88.08% in the presence of humic acid (Figure S4). However, PS_{NaOH} demonstrated good removal efficiency of BG in the presence of different ions (except $CaCl_2$) and organic matter, highlighting its practical applicability in wastewater treatment.

2.4. Molecular Modeling and Docking

Molecular modeling is a pivotal tool for performing simulations at the atomistic level to explore conformational geometries and electronic structures, as well as to grasp intra- and intermolecular interactions.

Brilliant green (BG), also known under various synonyms (malachite green G, basic green 1, and emerald green) is an organic hydrogen sulfate salt having 4-[[4-(diethylamino) phenyl](phenyl)methylidene}-N,N-diethylcyclohexa-2,5-dien-1-iminium ($C_{27}H_{33}N_2^+$) as the counterion [65]. Computational results (by DFT) for the BG molecule (in its cationic form) are summarized in the Supplementary Materials (Figure S5 and Table S7).

In the subsequent molecular modeling procedures, the BG molecule (cationic form) was considered the ligand for molecular docking computations. To this end, its optimized geometry (at the DFT level) was taken as the starting structure for these simulations. Likewise, for the molecular docking computations, we considered two receptors: (1) cellulose oligomer (cellotetraose) and (2) lignin. The outcomes of the molecular docking are illustrated in Figures 5 and 6 for the cellotetraose receptor and lignin receptor, respectively. In these figures, the best poses of the docked complexes are given, detailing the intermolecular interactions between the ligand (BG) and receptors. As shown in Figure 5, the hydrogen bonds (H-bonds) are present inside the cellotetraose receptor (intramolecular interactions) and are rendered as dotted yellow lines. The intermolecular interactions between cellotetraose and the BG molecule rely on hydrophobic contacts (highlighted in Figure 5 as solid green lines). These hydrophobic contacts can be correlated with the physical adsorption (on the basis of van-der-Waals forces) of BG dye onto cellulose. Computational results revealed for the docked complex cellotetraose–BG a binding energy (E_b) of -2.84 kcal/mol and a dissociation constant (K_d) equal to 8.27 mM. The large value of the dissociation constant ($K_d = 8.27$ mM) suggests that the interaction between the ligand and cellotetraose receptor is not strong and that the dissociation of the docked complex is possible.

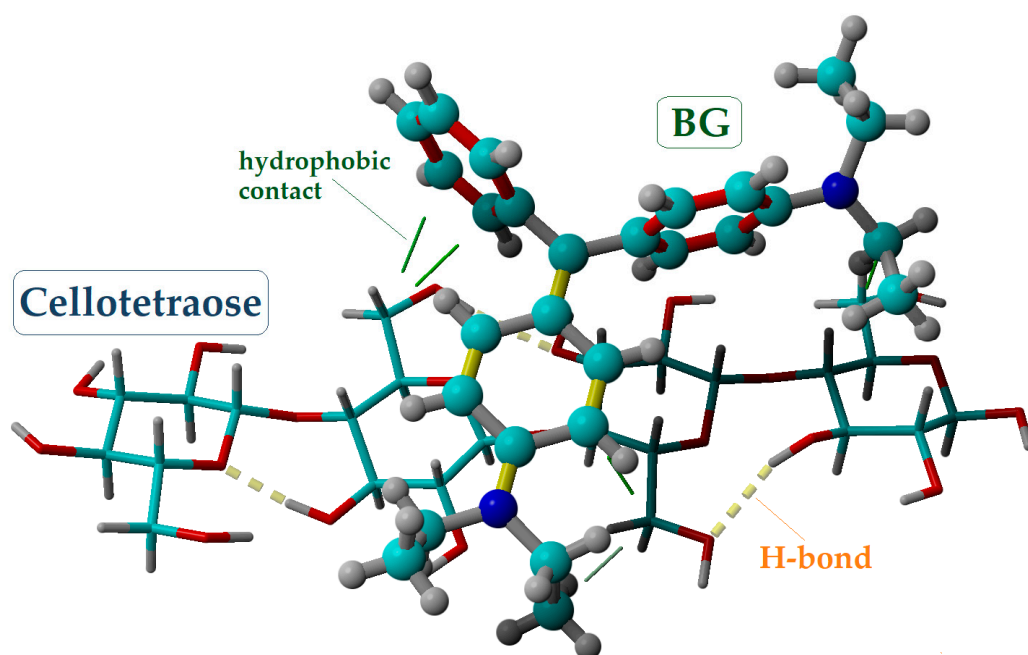


Figure 5. Molecular docking outcomes, showing the best pose of the docked complex between cellotetraose receptor and BG ligand, as well as their interaction mode; $E_b = -2.84$ kcal/mol and $K_d = 8.27$ mM.

For the second case, the docked complex lignin–BG is illustrated in Figure 6. Compared to the previous complex (cellotetraose–BG), the interaction between the lignin receptor and BG ligand was stronger, disclosing lower values for the affinity parameters (i.e., $E_b = -4.59$ kcal/mol and $K_d = 0.43$ mM). Moreover, molecular docking results indicated that, for this case, beyond the hydrophobic contacts, π – π stacking interactions can emerge between the lignin and BG (rendered in Figure 6 as red lines). These types of interactions (π – π stacking) refer to the presumptive attractive, non-covalent interactions (orbital overlap) between the π bonds of aromatic rings. The π – π interactions might be associated with

chemisorption. It should be mentioned that the simulations also revealed intramolecular H-bond formation in the conformation of the lignin receptor (Figure 6).

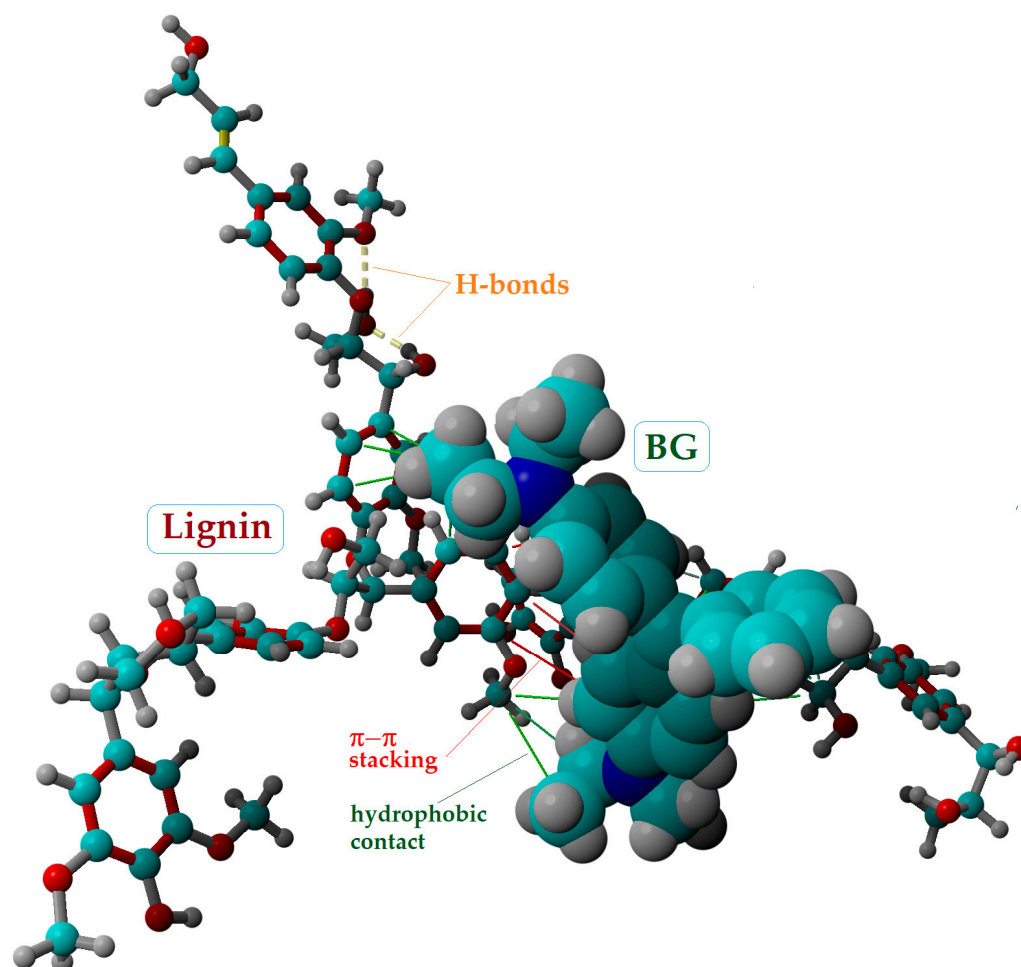


Figure 6. Molecular docking outcomes, showing the best pose of the docked complex between lignin receptor and BG ligand, and their interaction mode; $E_b = -4.59$ kcal/mol and $K_d = 0.43$ mM.

In addition, the interaction energies between the ligand (BG) and receptors (cellotetraose and lignin) were calculated at the level of the YASARA force field in order to account for the contributions of the van-der-Waals and Coulomb forces. In this respect, the interaction energy (ΔE) between the ligand and receptor (relying on the molecular force field) was calculated according to [66]

$$\Delta E = E_{\text{COMPLEX}} - (E_{\text{RECEPTOR}} + E_{\text{LIGAND}}) \quad (9)$$

where ΔE is the energy of interaction between the ligand and receptor, E_{COMPLEX} denotes the potential energy of the docked complex, E_{RECEPTOR} is the potential energy of the receptor, and E_{LIGAND} is the potential energy of the ligand. Note that each term (from Equation (9)) includes both intramolecular and intermolecular contributions. The latter one involves two individual energy components for van-der-Waals (vdW) and Coulomb forces, which are responsible for distance-dependent attractive/repulsive interactions and electrostatic effects, respectively [66]. In general, the lower the interaction energy, the stronger the interaction between the ligand and receptor.

Table 4 gives the energies of intermolecular interactions between the BG dye (ligand) and both receptors. As reported in Table 4, the interaction between BG and cellotetraose is based principally on vdW forces ($\Delta E_{\text{vdW}} = -9.00$ kcal/mol). In turn, the electrostatic interactions for the cellotetraose–BG complex are minor ($\Delta E_{\text{CL}} = -0.97$ kcal/mol). For

the second case of lignin binding with BG, the major role is attributed to electrostatic interactions ($\Delta E_{CL} = -21.30$ kcal/mol), whereas the vdW forces ($\Delta E_{vdW} = -8.21$ kcal/mol) were of secondary importance. The docking results for the lignin–BG system were in good agreement with the D-R isotherm results that suggested a mechanism of adsorption based on ion exchange (i.e., electrostatic interactions). The overall intermolecular interaction energy ($\Delta E = \Delta E_{vdW} + \Delta E_{CL}$) was lower for the lignin–BG complex (Table 4), indicating that the ligand (BG dye) interacted more strongly with lignin compared to cellotetraose.

Table 4. Energy of intermolecular interactions between BG cationic dye (ligand) and receptors (cellotetraose and lignin) calculated at the level of the YASARA force field.

Docking System (Ligand–Receptor)	Total Intermolecular: $\Delta E = \Delta E_{vdW} + \Delta E_{CL}$ (kcal/mol)	van-der-Waals: ΔE_{vdW} (kcal/mol)	Coulomb: ΔE_{CL} (kcal/mol)
Cellotetraose–BG	−9.97	−9.00	−0.97
Lignin–BG	−29.51	−8.21	−21.30

3. Materials and Methods

3.1. Materials

Brilliant green (BG) and sodium hydroxide $\geq 97.0\%$ were purchased from Merck Chemical (Saint Louis, MO, USA). A stock experimental solution of BG cationic dye was prepared by using distilled water (concentration of 1 g/L). The pistachio shells (acquired from a local grocery store) were subjected to mechanical grinding using a Pulverisette 11 knife mill (Fritsch, Idar-Oberstein, Germany) after pre-washing with distilled water and drying at 378 K in a laboratory oven. Pistachio shells (PS) were further subjected to an alkaline treatment by being immersed in a 5% NaOH aqueous solution and magnetically stirred (150 rpm) for 48 h at room temperature. The final alkali-treated PS_{NaOH} biosorbent was produced after the grains were filtered, thoroughly rinsed with bi-distilled water (to remove excess sodium hydroxide), and dried at 338 K for 24 h in an oven. Grains with sizes between 0.5 and 1.5 mm were obtained (Figure S6 in the Supplementary Materials).

3.2. PS_{NaOH} Biosorbent Characterization

The surface morphological properties of the alkali-treated biosorbent were examined using a Quanta 200 Scanning Electron Microscope (Brno, Czech Republic). A structural investigation was performed using a Bruker Vertex 70 Fourier Transform Infrared Spectrophotometer (Ettlingen, Germany) in the range of 4000–600 cm^{-1} in attenuated total reflectance mode (2 cm^{-1} resolution and 64 scans). Brilliant green adsorption onto the PS_{NaOH} biosorbent was evidenced using a polarized optical microscope (Leica Microsystems, Wetzlar, Germany). The water vapor sorption capacities of the PS and PS_{NaOH} samples were determined in the dynamic regime by using IGA sorp fully automated gravimetric equipment (Hidden Analytical, Warrington, UK).

3.3. Adsorption of Brilliant Green onto PS_{NaOH} Biosorbent

Brilliant green adsorption onto the PS_{NaOH} biosorbent was employed by using an orbital shaker incubator, the Biosan ES-20/60 (Riga, Latvia). A Hitachi U-3900 dual-beam UV–VIS spectrophotometer (Hitachinaka, Japan) was used to measure the dye content in the aqueous solutions, using previously determined calibration curves and the detection of adsorption bands (318, 426, and 624 nm), as depicted in Figure S1.

Kinetic experiments were carried out in batch mode to determine the adsorption capacity of the sorbent over time ($T = 300$ K). Thus, 0.2 g of PS_{NaOH} biosorbent was introduced in 50 mL of 50 mg/L BG solution (orbital shaker, 180 rpm, 4 h). The dye concentration in the solution was determined by taking aliquots from the dye solutions at

various predetermined contact times. The adsorption kinetics as a function of time were calculated according to Equation (9):

$$q_t(\text{mg/g}) = \frac{(C_0 - C_t)V}{m \cdot 1000}, \quad (10)$$

where q_t (mg/g) is the amount of dye absorbed at time t (min); C_0 and C_t (mg/L) are the dye concentrations in the initial and final solutions (after contact time t), respectively; V (mL) is the volume of the immersion medium, and m (g) represents the weight of the PS_{NaOH} biosorbent.

The adsorption isotherms were measured at two different temperatures: 300 K and 330 K. As a result, for the same 0.2 g amount of biosorbent, the initial concentrations of the dye solutions ranged between 10 and 500 mg/L (contact time was set at 4 h, 180 rpm). The adsorption capacity at equilibrium (q_e , mg/g) was calculated based on Equation (9) (by introducing the C_e concentration at equilibrium instead of the C_t concentration at time t).

The effect of coexisting anions (Cl^- , NO_2^- , and SO_4^{2-}) and cations (Na^+ , Ca^{2+} , and Fe^{2+}) from different salt species was investigated in a 50 mL solution of 10 mg/L BG (with 200 mg/L of NaCl, CaCl₂, NaNO₂, or FeSO₄ salt content and a 4 g/L sorbent dose). Similarly, the effect of organic matter was evaluated using humic acid (20 mg/L).

3.4. Optimization of the Adsorption Process

The adsorption process' optimization was carried out by applying the design of experiments (DoE) and the response surface methodology (RSM) [63,64]. Brilliant green dye (BG) was used as a model organic pollutant and was dissolved in an aqueous medium. The experiments were done at a temperature of 300 K and at a naturally occurring pH of 6.0 ± 0.2 . The adsorption performance was quantified via the color removal efficiency Y (response of the process), which was determined experimentally after a contact time of 120 min. The aim of the optimization was to maximize the color removal efficiency Y (%), which can be expressed as

$$Y(\%) = \left(1 - \frac{C_t}{C_0}\right) \times 100, \quad (11)$$

where C_0 denotes the initial concentration of the BG dye (organic pollutant), and C_t is the residual concentration of the BG dye determined after a contact time of $t = 120$ min. For modeling purposes, the sorbent dose (SD , g/L) and initial pollutant concentration C_0 (mg/L) were investigated as the main factors and were transformed into coded (dimensionless) variables x_1 and x_2 . This conversion was carried out to compare the effects of the factors using the same dimensionless scale. The mathematical relationships adopted for the conversion of actual factors into coded variables have been detailed by others [63,64].

3.5. Molecular Modeling of Brilliant Green Cationic Dye

The initial 3D conformer of BG, in its cationic form ($\text{C}_{27}\text{H}_{23}\text{N}_2^+$), was downloaded from the PubChem database [65] (PubChem CID 12449) and then subjected to molecular modeling at the level of density functional theory (DFT). The molecular modeling simulations were performed on a Dell Precision workstation T7910 with 32 CPU threads.

The quantum chemical calculations by the DFT method were carried out using the Gaussian16 software package [67]. The density functional with spherical atom dispersion terms APFD [68] was applied in this case by considering a split-valence (triple-zeta) basis set with polarization functions, i.e., APFD/6-311G(2d,p). The outcomes of DFT simulations were visualized and analyzed using the GaussView 6 program [69].

3.6. Molecular Docking

The molecular docking simulations were performed by using the AutoDock VINA algorithm [70] inbuilt into the YASARA-Structure program (v.20.8.23) for modeling and visualization [71,72]. The molecular conformation of the first receptor (cellulose oligomer) was optimized at the level of the YASARA force field, starting from the crystallographic

data of cellotetraose already reported [73]. Regarding the reference structure of lignin (the second receptor), this was retrieved from the PubChem platform [34] (PubChem CID: 73555271), and then it was subjected to a minor modification by adding a moiety ($-\text{COO}^-$) in order to simulate the presence of one carboxylic group. Subsequently, the conformation (3D structure) of this second receptor was subjected to energy minimization (for geometry optimization) at the level of the YASARA force field. Molecular docking simulations were carried out in the YASARA-Structure program environment. In this regard, for each system, a total of 100 docking poses were assayed at the level of molecular mechanics theory using the YASARA force field. In the course of the molecular docking simulations, the ligand (BG molecule) was treated as a flexible body, while both receptors were treated as rigid bodies. The parameters for the modeled structures were generated automatically by means of the algorithm "AutoSMILES" included in the YASARA-Structure program.

4. Conclusions

Pistachio shells (lignocellulosic waste) were subjected to grinding and alkaline treatment to obtain an efficient, low-cost biosorbent (PS_{NaOH}). The morphological and structural modifications were explored via the SEM, FTIR, and PoLM characterization techniques. Brilliant green (BG) cationic dye was used in the adsorption experiments as a hazardous organic pollutant dissolved in water. The investigated adsorption process followed pseudo-first-order (PFO) kinetics. The experimental data on adsorption isotherms revealed a maximum adsorption capacity of 52.42 mg/g at 300 K. The Sips isotherm model provided the best accuracy of data interpolation. The values of the mean free energy of sorption (E_s , resulting from the Dubinin–Radushevich isotherm) were around 13.1 kJ/mol, indicating that the adsorption mechanism was mainly based on ion exchange.

Two approaches were applied to assess the adsorption equilibrium constant (K_{ad}) and, consequently, the thermodynamic parameters. Both methods revealed similar results regarding the values of thermodynamic parameters. For the approach relying on the revised Langmuir isotherm model, there is no need to compute the activity coefficient. The negative values for the Gibbs free energy ($\Delta G_{ad} < 0$) and for the enthalpy ($\Delta H_{ad} < 0$) indicated that the studied adsorption processes were spontaneous and exothermic.

The process optimization based on the response surface methodology (RSM) indicated the optimal conditions for the adsorption of BG onto the PS_{NaOH} (i.e., $SD = 4.0$ g/L and $C_0 = 10.1$ mg/L). The experimental results confirmed that under the optimal conditions established, the effective removal efficiency was $Y = 98.78\%$, which was the maximum value observed in this study.

The outcomes of the molecular docking computations revealed the possible intermolecular interactions between lignocellulosic receptors (cellulose oligomer or lignin) and the BG molecule. For the cellotetraose–BG docked complex, the interactions were based mainly on hydrophobic contacts (vdW forces). Instead, the lignin–BG docked complex was stabilized by hydrophobic contacts, π – π stacking, and electrostatic (Coulomb) interactions.

Supplementary Materials: The following supporting information can be downloaded at: <https://www.mdpi.com/article/10.3390/molecules28104129/s1>, Figure S1: (a) Determination of maximum absorbance wavelengths for brilliant green cationic dye; (b) Calibration curve graphical representation of at a wavelength of 624 nm (concentration range of 0–10 mg/L); Figure S2: Adsorption isotherm data fitted to the revised Langmuir isotherm model (Azizian approach [36]), showing the adsorption equilibrium established between the surface of pistachio shell adsorbent and brilliant green (BG) cationic dye; water solubility of BG dye is $C_s = 1 \times 10^5$ mg/L.; Figure S3: Effect of pH: removal efficiency of brilliant green (BG) from aqueous solutions of pH 2 and 4 (adjusted with 0.1 M H_2SO_4) and pH 8 and 10 (adjusted with 0.1 M NaOH) compared to natural pH 6; optimal experimental conditions: $SD = 4$ g/L, $C_0 = 10$ mg/L, $V = 50$ mL, $t = 240$ min); Figure S4: Removal efficiency of brilliant green (BG) from aqueous solutions in the presence of different salts (200 mg/L NaCl, CaCl_2 , NaNO_2 , or FeSO_4), and in the presence of organic matter (20 mg/L humic acid); optimal experimental conditions: $SD = 4$ g/L, $C_0 = 10$ mg/L, $V = 50$ mL, $t = 240$; Figure S5: Molecular structure and particularities of BG molecule estimated computationally at DFT/APFD/6-311G(2d,p)

level of theory for ground state S_0 (charge = +1, singlet): (a) optimized geometry and dipole moment; (b) frontier molecular orbitals (HOMO, LUMO); (c) partial atomic charges (Mulliken) distribution; (d) electrostatic potential (ESP) map. Min; Figure S6: PS_{NaOH} grains image obtained by optical microscope (Conrad USB, Wels, Austria); Table S1: FTIR spectra absorption band assignments for unmodified and alkali-treated pistachio shells (PS and PS_{NaOH} , respectively); Table S2: Surface parameters of PS and PS_{NaOH} samples evaluated based on dynamic vapor sorption measurements: water vapor sorption capacity, final weight (W); average pore size (p_s), surface area (A), and monolayer weight (W_m); Table S3: Kinetic model equations and parameters* for BG dye adsorption onto PS_{NaOH} biosorbent (experimental conditions: $T = 300$ K, sorbent dose = 4 g/L, $C_0 = 50$ mg/L); Table S4: Isotherm models (equations and parameters) for BG cationic dye adsorption onto PS_{NaOH} biosorbent ($t = 240$ min, sorbent dose = 4 g/L); Table S5: Parameters of the revised Langmuir isotherm model determined for BG dye adsorption onto PS_{NaOH} biosorbent ($CS = 1 \times 10^5$ mg/L (solubility for BG dye)); Table S6: Analysis of variance (ANOVA) for the multiple regression model $\hat{Y}(x_1, x_2)$; Table S7: Summary of molecular and global reactivity descriptors for BG molecule (cationic form); descriptors computed by DFT method at APFD/6-311G(2d,p) level of theory.

Author Contributions: Conceptualization, A.-C.E., C.C. and P.S.; methodology, A.-C.E., C.C. and P.S.; software, C.C.; validation, A.-C.E., C.C., P.S., V.C. and V.H.; formal analysis, V.C., R.A. and G.P.; investigation, A.-C.E., C.C. and P.S.; resources, P.S. and V.H.; writing—original draft preparation, A.-C.E. and C.C.; writing—review and editing, C.C., P.S. and V.H.; supervision, V.H.; project administration, P.S. and C.C.; funding acquisition, P.S. All authors have read and agreed to the published version of the manuscript.

Funding: The support of the European Regional Development Fund, Competitiveness Operational Programme 2014–2020, POC/163/1/3—Project 4WASTEUPGRADE (Contract No. 386/390062/04.10.2021, MySMIS code: 120696), is gratefully acknowledged.

Institutional Review Board Statement: Not applicable.

Informed Consent Statement: Not applicable.

Data Availability Statement: Not applicable.

Conflicts of Interest: The authors declare no conflict of interest.

Sample Availability: Not available.

References

1. Pratap, B.; Kumar, S.; Nand, S.; Azad, I.; Bharagava, R.N.; Ferreira, L.F.R.; Dutta, V. Wastewater generation and treatment by various eco-friendly technologies: Possible health hazards and further reuse for environmental safety. *Chemosphere* **2023**, *313*, Z37547. [[CrossRef](#)] [[PubMed](#)]
2. Slama, H.B.; Chenari Bouket, A.; Pourhassan, Z.; Alenezi, F.N.; Silini, A.; Cherif-Silini, H.; Oszako, T.; Luptakova, L.; Golińska, P.; Belbahri, L. Diversity of Synthetic Dyes from Textile Industries, Discharge Impacts and Treatment Methods. *Appl. Sci.* **2021**, *11*, 6255. [[CrossRef](#)]
3. Teo, S.H.; Ng, C.H.; Islam, A.; Abdulkareem-Alsultan, G.; Joseph, C.G.; Janaun, J.; Taufiq-Yap, Y.H.; Khandaker, S.; Islam, G.J.; Znad, H.; et al. Sustainable toxic dyes removal with advanced materials for clean water production: A comprehensive review. *J. Clean. Prod.* **2021**, *332*, 130039. [[CrossRef](#)]
4. Adnan, A.; Omer, M.; Khan, B.; Khan, I.; Alamzeb, M.; Zada, F.M.; Ullah, I.; Shah, R.; Alqarni, M.; Simal-Gandara, J. Equilibrium, Kinetic and Thermodynamic Studies for the Adsorption of Metanil Yellow Using Carbonized Pistachio Shell-Magnetic Nanoparticles. *Water* **2022**, *14*, 4139. [[CrossRef](#)]
5. Mansour, R.; Sameda, M.G.; Zaatout, A. Adsorption studies on brilliant green dye in aqueous solutions using activated carbon derived from guava seeds by chemical activation with phosphoric acid. *Desalination Water Treat.* **2020**, *202*, 396–409. [[CrossRef](#)]
6. Karanfil, D.Y.; Coşkun, R.; Delibaş, A. Aminated magnetic polymeric resin for removal of anthraquinone and azo dyes from aqueous solutions. *J. Polym. Res.* **2022**, *29*, 87. [[CrossRef](#)]
7. Singh, S.; Gupta, H.; Dhiman, S.; Sahu, N.K. Decontamination of cationic dye brilliant green from the aqueous media. *Appl. Water Sci.* **2022**, *12*, 61. [[CrossRef](#)]
8. Şentürk, I.; Alzein, M. Adsorptive removal of basic blue 41 using pistachio shell adsorbent—Performance in batch and column system. *Sustain. Chem. Pharm.* **2020**, *16*, 100254. [[CrossRef](#)]
9. Ghoniem, M.G.; Ali, F.A.M.; Abdulkhair, B.Y.; Elamin, M.R.A.; Alqahtani, A.M.; Rahali, S.; Ben Aissa, M.A. Highly Selective Removal of Cationic Dyes from Wastewater by MgO Nanorods. *Nanomaterials* **2022**, *12*, 1023. [[CrossRef](#)] [[PubMed](#)]
10. Nandi, B.K.; Goswami, A.; Purkait, M.K. Adsorption characteristics of brilliant green dye on kaolin. *J. Hazard. Mater.* **2009**, *161*, 387–395. [[CrossRef](#)] [[PubMed](#)]

11. Babalska, Z.L.; Korbecka-Paczkowska, M.; Karpiński, T.M. Wound Antiseptics and European Guidelines for Antiseptic Application in Wound Treatment. *Pharmaceuticals* **2021**, *14*, 1253. [[CrossRef](#)]
12. Mane, V.S.; Mall, I.D.; Srivastava, V.C. Use of bagasse fly ash as an adsorbent for the removal of brilliant green dye from aqueous solution. *Dyes. Pigm.* **2007**, *73*, 269–278. [[CrossRef](#)]
13. Mane, V.S.; Babu, P.V.V. Studies on the adsorption of Brilliant Green dye from aqueous solution onto low-cost NaOH treated saw dust. *Desalination* **2011**, *273*, 321–329. [[CrossRef](#)]
14. Pohanish, R.P. *Sittig's Handbook of Toxic and Hazardous Chemicals and Carcinogens*, 7th ed.; Elsevier Inc.: Oxford, UK, 2017; pp. 2791–2792.
15. El-Chaghaby, G.A.; Ramis, E.S.; Ahmad, A.F. Rice straw and rice straw ash for the removal of brilliant green dye from wastewater. *Asian J. Appl. Chem.* **2018**, *15*, 1–9. [[CrossRef](#)]
16. Opladowska, M.; Donnelly, R.F.; Majithiya, R.J.; Kennedy, D.G.; Elliott, C.T. The potential for human exposure, direct and indirect, to the suspected carcinogenic triphenylmethane dye Brilliant Green from green paper towels. *Food Chem. Toxicol.* **2011**, *49*, 1870–1876. [[CrossRef](#)]
17. Abbas, M. Removal of brilliant green (BG) by activated carbon derived from medlar nucleus (ACMN)—Kinetic, isotherms and thermodynamic aspects of adsorption. *Adsorp. Sci. Technol.* **2020**, *38*, 464–482. [[CrossRef](#)]
18. Kismir, Y.; Aroguz, A.Z. Adsorption characteristics of the hazardous dye Brilliant Green on Saklikent mud. *J. Chem. Eng.* **2011**, *172*, 199–206. [[CrossRef](#)]
19. Przysaś, W.; Zabłocka-Godlewska, E.; Grabińska-Sota, E. Biological Removal of Azo and Triphenylmethane Dyes and Toxicity of Process By-Products. *Water Air Soil Pollut.* **2012**, *223*, 1581–1592. [[CrossRef](#)]
20. Rehman, F.; Sayed, M.; Khan, J.A.; Shah, N.S.; Khan, H.M.; Dionysiou, D.D. Oxidative removal of brilliant green by UV/S₂O₈²⁻, UV/HSO₅⁻ and UV/H₂O₂ processes in aqueous media: A comparative study. *J. Hazard. Mater.* **2018**, *357*, 506–514. [[CrossRef](#)] [[PubMed](#)]
21. Mariah, G.K.; Pak, K.S. Removal of brilliant green dye from aqueous solution by electrocoagulation using response surface methodology. *Mater. Today Proc.* **2020**, *20*, 488–492. [[CrossRef](#)]
22. Mukhopadhyay, A.; Tripathy, B.K.; Debnath, A.; Kumar, M. Enhanced persulfate activated sono-catalytic degradation of brilliant green dye by magnetic CaFe₂O₄ nanoparticles: Degradation pathway study, assessment of bio-toxicity and cost analysis. *Surf. Interfaces* **2021**, *26*, 101412. [[CrossRef](#)]
23. Sharma, N.; Purkait, M.K. Enantiomeric and racemic effect of tartaric acid on polysulfone membrane during crystal violet dye removal by MEUF process. *J. Water Process. Eng.* **2016**, *10*, 104–112. [[CrossRef](#)]
24. Samiyammal, P.; Kokila, A.; Pragasan, L.A.; Rajagopal, R.; Sathya, R.; Ragupathy, S.; Krishnakumar, M.; Minnam Reddy, V.R. Adsorption of brilliant green dye onto activated carbon prepared from cashew nut shell by KOH activation: Studies on equilibrium isotherm. *Environ. Res.* **2022**, *212*, 113497. [[CrossRef](#)]
25. Ghaedi, M.; Hossainian, H.; Montazerzohori, M.; Shokrollahi, A.; Shojai pour, F.; Soylak, M.; Purkait, M.K. A novel acorn based adsorbent for the removal of brilliant green. *Desalination* **2011**, *281*, 226–233. [[CrossRef](#)]
26. Enache, A.-C.; Samoila, P.; Cojocaru, C.; Apolzan, R.; Predeanu, G.; Harabagiu, V. An Eco-Friendly Modification of a Walnut Shell Biosorbent for Increased Efficiency in Wastewater Treatment. *Sustainability* **2023**, *15*, 2704. [[CrossRef](#)]
27. Sun, Y.; Wang, T.; Han, C.; Bai, L.; Sun, X. One-step preparation of lignin-based magnetic biochar as bifunctional material for the efficient removal of Cr(VI) and Congo red: Performance and practical application. *Bioresour. Technol.* **2023**, *369*, 128373. [[CrossRef](#)]
28. Sun, Y.; Wang, T.; Han, C.; Lv, X.; Bai, L.; Sun, X.; Zhang, P. Facile synthesis of Fe-modified lignin-based biochar for ultra-fast adsorption of methylene blue: Selective adsorption and mechanism studies. *Bioresour. Technol.* **2022**, *344*, 126186. [[CrossRef](#)] [[PubMed](#)]
29. Bushra, R.; Mohamad, S.; Alias, Y.; Jin, Y.; Ahmad, M. Current approaches and methodologies to explore the perceptive adsorption mechanism of dyes on low-cost agricultural waste: A review. *Microporous Mesoporous Mater.* **2021**, *319*, 111040. [[CrossRef](#)]
30. Khezri, M.; Heerema, R.; Brar, G.; Ferguson, L. Alternate bearing in pistachio (*Pistacia vera* L.): A review. *Trees* **2020**, *34*, 855–868. [[CrossRef](#)]
31. Taghizadeh, A.; Rad-Moghadam, K. Green fabrication of Cu/pistachio shell nanocomposite using Pistacia Vera L. hull: An efficient catalyst for expedient reduction of 4-nitrophenol and organic dyes. *J. Clean. Prod.* **2018**, *198*, 1105–1119. [[CrossRef](#)]
32. Mandalari, G.; Barreca, D.; Gervasi, T.; Roussel, M.A.; Klein, B.; Feeney, M.J.; Carughi, A. Pistachio Nuts (*Pistacia vera* L.): Production, Nutrients, Bioactives and Novel Health Effects. *Plants* **2022**, *11*, 18. [[CrossRef](#)]
33. Pumilia, G.; Cichon, M.J.; Cooperstone, J.L.; Giuffrida, D.; Dugo, G.; Schwartz, S.J. Changes in chlorophylls, chlorophyll degradation products and lutein in pistachio kernels (*Pistacia vera* L.) during roasting. *Int. Food Res. J.* **2014**, *65*, 193–198. [[CrossRef](#)]
34. Huang, J.; Fu, S.; Gan, L. *Lignin Chemistry and Applications*; Elsevier: Amsterdam, The Netherlands, 2019; pp. 25–37.
35. Aki, M.A.; Mostafa, M.M.; Bashanaini, M.S.A. Enhanced Removal of Some Cationic Dyes from Environmental Samples Using Sulphuric Acid Modified Pistachio Shells Derived Activated Carbon. *J. Chromatogr. Sep. Tech.* **2016**, *7*, 329. [[CrossRef](#)]
36. Azizian, S.; Eris, S.; Wilson, L.D. Re-evaluation of the century-old Langmuir isotherm for modeling adsorption phenomena in solution. *Chem. Phys.* **2018**, *513*, 99–104. [[CrossRef](#)]
37. Akbarpour, R.; Rasooli, A.; Salimi, H.; Mahroudi, A. Using Pistachio Agricultural Waste to Remove Environmental Pollutants: A Review Study. *Pistachio Health J.* **2022**, *5*, 40–48. [[CrossRef](#)]

38. Zafeiropoulos, N.E. Engineering the fibre—Matrix interface in natural-fibre composites. In *Properties and Performance of Natural-Fibre Composites*; Pickering, K.L., Ed.; Woodhead Publishing Limited: Cambridge, UK, 2008; pp. 127–162. [CrossRef]
39. Ferro, M.; Mannu, A.; Panzeri, W.; Theeuwes, C.H.J.; Mele, A. An Integrated Approach to Optimizing Cellulose Mercerization. *Polymers* **2020**, *12*, 1559. [CrossRef]
40. Khan, M.A.; Al Othman, Z.A.; Kumar, M.; Ola, M.S.; Siddique, M.R. Biosorption potential assessment of modified pistachio shell waste for methylene blue: Thermodynamics and kinetics study. *Desalin. Water Treat.* **2014**, *56*, 146–160. [CrossRef]
41. Popescu, M.-C.; Popescu, C.-M.; Lisa, G.; Sakata, Y. Evaluation of morphological and chemical aspects of different wood species by spectroscopy and thermal methods. *J. Mol. Struct.* **2011**, *988*, 65–72. [CrossRef]
42. Javier-Astete, R.; Jimenez-Davalos, J.; Zolla, G. Determination of hemicellulose, cellulose, holocellulose and lignin content using FTIR in *Calycophyllum spruceanum* (Benth.) K. Schum. and *Guazuma crinita* Lam. *PLoS ONE* **2021**, *16*, e0256559. [CrossRef] [PubMed]
43. Mustikaningrum, M.; Cahyono, R.B.; Yuliansyah, A.T. Effect of NaOH Concentration in Alkaline Treatment Process for Producing Nano Crystal Cellulose-Based Biosorbent for Methylene Blue. *IOP Conf. Ser. Mater. Sci. Eng.* **2021**, *1053*, 012005. [CrossRef]
44. Chambre, D.R.; Dochia, M. FT-IR characterization of cellulose crystallinity from raw bast fibers. *Scien. Tech. Bull.-Chem. Food Sci. Eng.* **2021**, *18*, 10–17.
45. Agwuncha, S.C.; Owonubi, S.; Fapojuwo, D.P.; Abdulkarim, A.; Okonkwo, T.P.; Makhatha, E.M. Evaluation of mercerization treatment conditions on extracted cellulose from shea nut shell using FTIR and thermogravimetric analysis. *Mater. Today Proc.* **2020**, *38*, 958–963. [CrossRef]
46. Humelnicu, A.-C.; Samoila, P.; Cojocaru, C.; Dumitriu, R.; Bostanaru, A.-C.; Mares, M.; Harabagiu, V.; Simionescu, B.C. Chitosan-Based Therapeutic Systems for Superficial Candidiasis Treatment. Synergetic Activity of Nystatin and Propolis. *Polymers* **2022**, *14*, 689. [CrossRef]
47. Bouziane, N.; Aloui, A.; Behloul, S.; Zertal, A. Kinetic models of aqueous 2-mercaptobenzothiazole adsorption on local clay and activated carbon. *Rev. Roum. Chim.* **2021**, *66*, 479–491.
48. Baidya, K.S.; Kumar, U. Adsorption of Brilliant green dye from aqueous solution onto chemically modified areca nut husk. *S. Afr. J. Chem. Eng.* **2020**, *35*, 33–43. [CrossRef]
49. Nguyen, T.H.A.; Pham, T.T. Brilliant Green Biosorption from Aqueous Solutions on Okara: Equilibrium, Kinetic and Thermodynamic Studies. *J. Water Environ. Technol.* **2023**, *21*, 30–40. [CrossRef]
50. Ebelegi, A.; Ayawei, N.; Wankasi, D. Interpretation of Adsorption Thermodynamics and Kinetics. *Open J. Phys. Chem.* **2020**, *10*, 166–182. [CrossRef]
51. Yang, S.; Zhao, F.; Sang, Q.; Zhang, Y.; Chang, L.; Huang, D.; Mu, B. Investigation of 3-aminopropyltriethoxysilane modifying attapulgite for Congo red removal: Mechanisms and site energy distribution. *Powder Technol.* **2021**, *383*, 74–83. [CrossRef]
52. Cojocaru, C.; Samoila, P.; Pascariu, P. Chitosan-based magnetic adsorbent for removal of water-soluble anionic dye: Artificial neural network modeling and molecular docking insights. *Int. J. Biol. Macromol.* **2018**, *123*, 587–599. [CrossRef] [PubMed]
53. Karam, T.E.; Siraj, N.; Zhang, Z.; Ezzir, A.F.; Warner, I.M.; Haber, L.H. Ultrafast and nonlinear spectroscopy of brilliant green-based nanoGUMBOS with enhanced near-infrared emission. *J. Chem. Phys.* **2017**, *147*, 144701. [CrossRef] [PubMed]
54. Abbas, A.; Murtaza, S.; Shahid, K.; Munir, M.; Ayub, R.; Akber, S. Comparative study of Adsorptive removal of congo red and brilliant green dyes from water using peanut shell. *J. Sci. Res.* **2012**, *11*, 828–832.
55. Badr, S.M.; Samaka, S. Using agricultural waste as biosorbent for hazardous brilliant green dye removal from aqueous solutions. *J. Eng. Sci. Technol.* **2021**, *16*, 3435–3454.
56. Laskar, N.; Kumar, U. Removal of Brilliant Green dye from water by modified Bambusa Tulda: Adsorption isotherm, kinetics and thermodynamics study. *Int. J. Environ. Sci. Technol.* **2019**, *16*, 1649–1662. [CrossRef]
57. Qu, L.; Han, T.; Luo, Z.; Liu, C.; Mei, Y.; Zhu, T. One-step fabricated Fe₃O₄@C core-shell composites for dye removal: Kinetics, equilibrium and thermodynamics. *J. Phys. Chem. Solids* **2015**, *78*, 20–27. [CrossRef]
58. Ghosal, P.S.; Gupta, A.K. Determination of thermodynamic parameters from Langmuir isotherm constant-revisited. *J. Mol. Liq.* **2017**, *225*, 137–146. [CrossRef]
59. Liu, Y. Is the free energy change of adsorption correctly calculated? *J. Chem. Eng.* **2009**, *54*, 1981–1985. [CrossRef]
60. Khan, A.A.; Singh, R.P. Adsorption thermodynamics of carbofuran on Sn (IV) arsenosilicate in H⁺, Na⁺ and Ca²⁺ forms. *Colloids Surf.* **1987**, *24*, 33–42. [CrossRef]
61. Cojocaru, C.; Humelnicu, A.C.; Pascariu, P.; Samoila, P. Artificial neural network and molecular modeling for assessing the adsorption performance of a hybrid alginate-based magsorbent. *J. Mol. Liq.* **2021**, *337*, 116406. [CrossRef]
62. Soldatkina, L.; Yanar, M. Optimization of Adsorption Parameters for Removal of Cationic Dyes on Lignocellulosic Agricultural Waste Modified by Citric Acid: Central Composite Design. *ChemEngineering* **2023**, *7*, 6. [CrossRef]
63. Bezerra, M.A.; Santelli, R.E.; Oliveira, E.P.; Villar, L.S.; Escalera, L.A. Response surface methodology (RSM) as a tool for optimization in analytical chemistr. *Talanta* **2008**, *76*, 965–977. [CrossRef]
64. Mäkelä, M. Experimental design and response surface methodology in energy applications: A tutorial review. *Energy Convers. Manag.* **2017**, *151*, 630–640. [CrossRef]
65. PubChem Database, National Library of Medicine, National Center for Biotechnology. Available online: <https://pubchem.ncbi.nlm.nih.gov/> (accessed on 9 February 2023).

66. Cojocaru, C.; Humelnicu, A.-C.; Samoila, P.; Pascariu, P.; Harabagiu, V. Optimized formulation of NiFe₂O₄@Ca-alginate composite as a selective and magnetic adsorbent for cationic dyes: Experimental and modeling study. *React. Funct. Polym.* **2018**, *125*, 57–69. [[CrossRef](#)]
67. Frisch, M.J.; Trucks, G.W.; Schlegel, H.B.; Scuseria, G.E.; Robb, M.A.; Cheeseman, J.R.; Scalmani, G.; Barone, V.; Mennucci, B.; Petersson, G.A.; et al. *Gaussian 09*; Gaussian Inc.: Wallingford, CT, USA, 2009; Available online: <http://www.gaussian.com/> (accessed on 10 February 2023).
68. Austin, A.; Petersson, G.A.; Frisch, M.J.; Dobek, F.J.; Scalmani, G.; Throssell, K. A density functional with spherical atom dispersion terms. *J. Chem. Theory Comput.* **2012**, *8*, 4989–5007. [[CrossRef](#)]
69. Dennington, R.; Keith, T.A.; Millam, J.M. *GaussView, Version 6.1*; Semichem Inc.: Shawnee Mission, KS, USA, 2016; Available online: <https://gaussian.com/gaussview6/> (accessed on 10 February 2023).
70. Trott, O.; Olson, A.J. AutoDock Vina: Improving the speed and accuracy of docking with a new scoring function, efficient optimization, and multithreading. *J. Comput. Chem.* **2010**, *31*, 455–461. [[CrossRef](#)]
71. Krieger, E.; Koraimann, G.; Vriend, G. Increasing the precision of comparative models with YASARA NOVA—A selfparameterizing force field. *Proteins* **2002**, *47*, 393–402. [[CrossRef](#)]
72. Krieger, E.; Vriend, G. YASARA View—molecular graphing for all devices—from smartphones to workstations. *Bioinformatics* **2014**, *30*, 2981–2982. [[CrossRef](#)] [[PubMed](#)]
73. Gessler, K.; Krauss, N.; Steiner, T.; Betzel, C.; Sarko, A.; Saenger, W. β-D-Cellotetraose Hemihydrate as a Structural Model for Cellulose II. An X-ray Diffraction Study. *J. Am. Chem. Soc.* **1995**, *117*, 11397–11406. [[CrossRef](#)]

Disclaimer/Publisher’s Note: The statements, opinions and data contained in all publications are solely those of the individual author(s) and contributor(s) and not of MDPI and/or the editor(s). MDPI and/or the editor(s) disclaim responsibility for any injury to people or property resulting from any ideas, methods, instructions or products referred to in the content.